IIETA International Information and Engineering Technology Association
Advancing the World of Information and Engineering

Revue des Composites et des Matériaux Avancés-Journal of Composite and Advanced Materials
Vol. 35, No. 6, December, 2025, pp. 1141-1152
Journal homepage: http://iieta.org/journals/rcma

Performance Optimization of Composite Pylons in Transtibial Prostheses Using Nanoparticles SIO_2: A Comparative Experimental and Numerical Study

Hussam Hussein Almusawi*, Majid Habeeb Faidh-Allah

Mechanical Engineering Department, College of Engineering, University of Baghdad, Baghdad 10071, Iraq

Corresponding Author Email: hossam.ali2303@coeng.uobaghdad.edu.iq

https://doi.org/10.18280/rcma.350614

Received: 6 November 2025
Revised: 7 December 2025
Accepted: 25 December 2025
Available online: 31 December 2025

Keywords:
prosthetic pylon, nanocomposite materials, glass fibers, Perlon fibers, resin, SIO_2, bagging vacuum device, FEM analysis

ABSTRACT

This paper addresses the research gap. Many studies have addressed the addition of nanomaterials, but none have examined their impact on the manufacture of prosthetic limbs, particularly those made of prosthetic pylon. It aims to evaluate the mechanical and physical effects of adding silicon dioxide (SIO_2) nanoparticles to a hybrid composite material consisting of glass fibers, Perlon and a polyester matrix. The novelty of this work using nanoparticles SIO_2 for enhancing composite materials for manufacturing prosthtic. Methodologically, two experimental sets were fabricated: a reference specimen (Δ1) and a nano-specimen (Δ2), using a vacuum-assisted resin infusion technique. The mechanical properties were characterized through tensile and flexural tests, and the structural performance was then evaluated through an experimental buckling test of the critical buckling load of the pylon for material (Δ2), which was improved by approximately 65% after the addition of SIO_2 compared to the material (Δ1). The results were compared with a theoretical model and a finite element model (FEM) built in ANSYS to simulate the critical mid-stance phase of the gait cycle. The results demonstrated a clear superiority of the nanomaterial, with the ultimate tensile strength increasing by more than 41% and the elastic modulus by nearly 54.4% compared to the reference sample. Furthermore, the manufactured pylon was 44% lighter and 40% less expensive to manufacture compared to its Al-6061 counterpart.

1. INTRODUCTION

The pylon is an essential component in below-knee amputee prosthetics. It supports the entire body weight and transfers dynamic loads during movement, ensuring the user's stability and structural integrity. Historically, traditional metallic materials such as titanium alloys, aluminum, and stainless steel have been used to manufacture this component. However, these materials, while strong, are often expensive and dense, and their excessive stiffness limits the prosthesis's ability to store and return kinetic energy, negatively impacting the user's smooth gait [1]. In this context, researcher Thurston developed a prototype prosthetic pylon using a combination of fiberglass and composite resin as an alternative to the traditional rigid below-the-knee pylon. This design is flexible enough to store energy during walking, improving the mobility of amputees [2]. Coleman also conducted a study comparing two pylons, one made of nylon (more flexible) and the other of aluminum (more rigid). The results showed that the nylon pylons provided greater comfort and ease of movement, enabling the user to walk faster than the rigid pylons [3]. In an effort to reduce costs, researcher Shasmin proposed using bamboo as an alternative to traditional materials (Ti, St, or Al) in the manufacture of artificial towers. Mechanical tests (tensile, bending, and compression) showed that bamboo possesses higher strength than aluminum and a modulus of elasticity suitable for the application [4]. For his part, Mohsen Jweeg studied the mechanical properties of an artificial pylon composed of carbon fiber reinforced with varying numbers of Perlon layers and an acrylic matrix. The results of tensile, fatigue, and impact tests showed that increasing the number of Perlon layers led to improved mechanical properties of the tower [5]. Priyadarsini et al. [6] performed a numerical and experimental analysis of the buckling of multilayer cylinders made of carbon fiber reinforced polymers (CFRP) using the finite element method (FEM). They studied the effect of loading characteristics, laminate geometrical placement, and defect size on buckling behavior. Jadhav and Gunjavate [7] also conducted a comparative study of differently oriented glass fiber laminates and found that the critical buckling load increased as the difference between the fiber orientation and the load direction decreased. Jawad K. Oleiwi and Shaima J. Ahmed investigated the tensile and buckling properties of a jute fiber-reinforced composite material, evaluating the effect of the number of layers and fiber angle (±45° and 0°/90°) on the mechanical performance [8]. More importantly, the potential of integrating nanotechnology to achieve simultaneous improvements in strength and stiffness remains a clear research gap in this field. Therefore, this study aims to bridge this gap by investigating the mechanical effect of

adding silicon dioxide nanoparticles (SiO_2) to a polyester composite matrix reinforced with a hybrid structure of three layers of glass fibers and six layers of Perlon fibers. The performance of this proposed nanocomposite material will be evaluated through experimental and numerical studies to determine its tensile and flexural properties of samples fabricated from this materials, as well as its critical buckling load for prosthetic pylon experimentally, numerically and theoretically, with the goal of developing a pylon design that combines light weight, high strength, and outstanding mechanical performance for below-knee prosthetic applications.

2. METHODOLOGY

The research methodology relied on the fabrication of samples to find mechanical properties for new materials when adding nanoparticles of SiO_2 [9] to composite materials consisting of glass fibers, Perlon fibers, and polyester resin as a binder. Two different formulations were prepared to evaluate mechanical performance and select the best one. The manufacturing process began with preparing a special plaster mold and installing a polyvinyl alcohol bag inside it. Then the fiberglass and Perlon layers were arranged at an angle of 0°/90°.

This was followed by injecting the resin mixed with nanoparticles using a vacuum technique at a pressure of up to 60 KPa to ensure material homogeneity and minimize air bubbles. After curing, the samples were cut to standard dimensions using a CNC machine. Mechanical tests, including tensile, bending, and buckling, were then conducted to evaluate the effect of incorporating the models. The results were used to select the best formulation, from which a final model was manufactured and subjected to numerical analysis using ANSYS Workbench 2023, with the aim of comparing the experimental results with finite element simulations. Figure 1 illustrates the sequence of steps involved in this methodology.

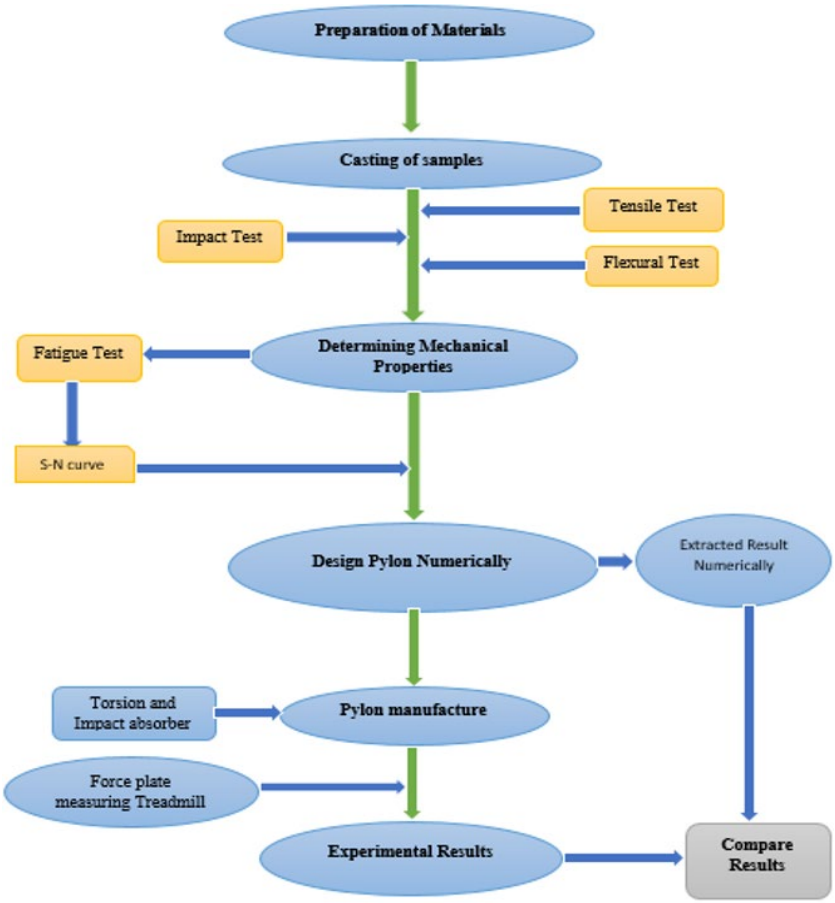

Figure 1. Methodology of fabrication prosthetic pylon

3. EXPERIMENTAL WORK

3.1 Proposed materials

For the purpose of this research, composite material samples were manufactured using reinforcing elements including glass fibers, Perlon fibers, and silicon dioxide nanoparticles (SiO_2) [10], with unsaturated polyester resin as a matrix material. Figure 2 shows the raw materials that are used in this study. To systematically investigate the effect of nanoparticles, two distinct experimental groups were prepared. The first composite material, denoted Δ1 served as the reference sample and consisted of a hybrid composite combining glass fibers and Perlon within a pure polyester resin matrix. As well as the second material, denoted as Δ2 represented the hybrid nanocomposite material, incorporating the same fiber architecture while reinforcing the polyester resin matrix with the percentage of nanoparticles (5%) [11]. In terms of laminate architecture, the reinforcement layers were arranged in groups (first and third) of Perlon fibers and in the middle glass fibers

to form a sequence of nine layers as follows:[perlon-3/glassfibers-3/perlon-3], i.e., three layers of Perlon, followed by three layers of glass fibers, then three more layers of Perlon.

(a) (b)

(c) (d)

Figure 2. Materials used in research

Figure 3. Vacuum bagging device

3.2 Sample manufacturing procedures

The composite specimens were manufactured using a gypsum mold measuring 30 × 20 × 5 cm³. To facilitate demolding and adhesion, the mold was lined with a polyvinyl alcohol (PVA) bag. The Perlon and glass fiber reinforcement layers were then placed inside the mold according to the specified stacking sequence for each material configuration, with fibers oriented at 0°/90°. After the mold was sealed with an outer PVA bag, a vacuum pump was used to extract air through a small vent port near the bottom of the mold.

In a separate step, the resin mixture was prepared by first mixing silicon dioxide nanoparticles into the polyester resin, then adding a hardener at a rate of 2% by weight of the resin. The mixture was then injected into the mold using the vacuum-assisted resin injection technique under a constant vacuum pressure of 60 KPa, as shown in Figure 3. This technique ensures homogeneous resin distribution and complete fiber saturation. Finally, after the hardening process was complete, the composite material was removed from the mold and the excess edges were trimmed. The manufacturing process of the composite material samples was carried out at a room temperature of 25°C.

Figure 4 displays a sample of the proposed composite material after finishing from manufacturing.

Figure 4. Sample of proposed composite materials

3.3 Characterization of the mechanical properties

To determine the basic mechanical properties of manufactured composite materials, two main tests were conducted on standard specimens: tensile testing and flexural testing. The tensile test aims to determine the intrinsic mechanical properties of the material, such as modulus of elasticity and ultimate tensile strength. The flexural test, on the other hand, measures the stiffness of the material and its ability to resist bending loads. The properties resulting from these two tests are essential inputs for the numerical model used to simulate the structural performance of the pylon.

3.3.1 Tensile test

A tensile test was conducted to determine the basic axial mechanical properties of the manufactured composite materials, according to ASTM D-3039 [12]. Specimens were prepared with nominal dimensions (250 mm × 25 mm × 4 mm), as shown in Figure 5. Tests were conducted using a UTD-50KN universal testing machine with a load capacity of 50 kN and a constant displacement speed of 1 mm/min at room temperature. The stress-strain curve was recorded for each specimen, from which the ultimate tensile strength, elongation at break, and Young's modulus were calculated. Three specimens were tested for each experimental group to ensure the reliability of the results. Figure 6 shows one of the specimens before being subjected to testing [13].

Figure 5. Samples of α1 before tensile test

Figure 6. Universal tensile test

Figure 7. Flexural test specimens

3.3.2 Test of flexural strength

The flexural properties of the composite materials were evaluated by performing a three-point bending test according to ASTM D790 [14]. Rectangular specimens with nominal dimensions of 100 mm (length) × 10 mm (width) × 4 mm (thickness) were tested as illustrated in Figure 7. The tests were conducted using a UTD-50KN universal testing machine, where the specimens were placed on supports with a span length of 80 mm, as shown in Figure 8. The load was applied at the center of the specimen at a constant displacement velocity of 1.25 mm/min. The load-deflection curve was recorded for each specimen, which was used to calculate both the flexural modulus and flexural strength.

Figure 8. Bending test device with specimen flexural

3.3.3 Fatigue test

Fatigue testing can provide valuable insights into the durability (service life) of the proposed material, especially since the socket is subjected to dynamic and varying stresses during the gait cycle. Conducting a fatigue test on composite materials is crucial for pylon engineering applications, as it indicates how well a material can endure cycles of loading and unloading during functional activities. Continuous loading can diminish the material's strength and elevate the likelihood of failure or fracture. Fatigue resistance poses significant challenges for materials with diverse properties [15]. Five meters with dimensions of 100 mm length, 10 mm width, and 4 mm thickness were used.

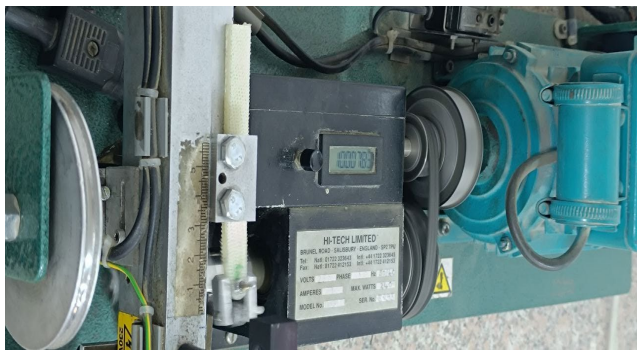

Figure 9. Device of fatigue test

Figure 9 shows a high-tech fatigue testing apparatus with a composite material sample attached. Using the first sample, the highest stress of 1886 MPa was applied, resulting in the sample breaking in a small number of cycles, not exceeding 60 cycles.

The deflection was fixed at 4 mm, and the highest stress from the tensile test, 188.6 MPa, was used (Figure 10).

Figure 10. Fatigue test specimens

4. MANUFACTURING OF PROSTHETIC PYLON

To evaluate the actual performance of the proposed composite material in practical applications, complete tower supports were fabricated from the (Δ1) and (Δ2) materials for buckling testing. The fabrication process began with the preparation of a stainless steel cylindrical rod as the filler, as shown in Figure 11, which was coated with a polyvinyl acetate (PVA) insulating layer. The reinforcement layers were then wrapped directly over the prepared rod in a hybrid stacking sequence [perlon-3/glassfibers-3/perlon-3].

Figure 11. Put glass fibers and Perlon around cylindrical rod

This hybrid arrangement was strategically designed to take advantage of the contrasting mechanical properties of each fiber type. The design relies on the high elastic modulus of glass fiber to provide the structural stiffness necessary to resist buckling loads. At the same time, the high toughness and elongation of Perlon fibers are utilized to provide the structure with a high capacity for absorbing impact energy and preventing brittle collapse. The outer Perlon layers also provide a high-quality surface finish as well as SIO_2. This arrangement was designed to achieve a targeted total volume fraction of approximately 30% for fibers with (8%) for glass fibers and (22%) for Perlon fibers and 70% for resin for (Δ1), and adding SIO_2 for type (Δ2).

After winding the fibers, this assembly was placed inside an external stainless-steel mold, sealed, and connected to a vacuum pump and resin supply. The resin system was prepared by adding a hardener to the polyester resin at a rate of 2% by weight. The resin was then drawn into the mold under vacuum for one hour to ensure complete saturation and curing, as shown in Figure 12.

Figure 12. Manufacturing pylons using vacuum bagging technique

Figure 13. Final shape of prosthetic pylon

Finally, after the curing was complete, the fabricated pylon was removed and prepared for structural testing, as shown in Figure 13.

The final shape of the pylon prosthesis, then weigh the prosthetic pylon using an electronic balance, illustrated in Figure 14.

Figure 14. Weight of manufactured pylon

5. COMPRESSION TEST

For estimate the theoretical critical buckling load of a pylon, Euler's equation was used as the basic reference value. The equation provides the relationship between the critical load and the geometric and mechanical properties of the pylon, as follows [16, 17]:

$$P_{cr} = \frac{\pi^2 EI}{L_{eff}} \quad (1)$$

To accurately apply this equation, the effective length (L_{eff}) must be determined based on support conditions that simulate the most critical operational condition. In the gait cycle, the highest axial compression loads on the prosthesis occur during the mid-stance phase, when the body weight is fully supported on one leg. At this stage, the lower limb of the pylon (the prosthetic foot side) can be modeled as a fixed limb due to its full contact with the ground, while the upper limb (the socket side) can be modeled as a pinned limb due to its ability to rotate. Based on these (fixed pinned) support conditions, the effective length of the pylon is calculated as ($L_e = 2L$), where L is the actual length of the pylon. The theoretical value of the critical load (P_{cr}) resulting from these conditions will be used in comparison with experimental and numerical results as shown in Figure 15.

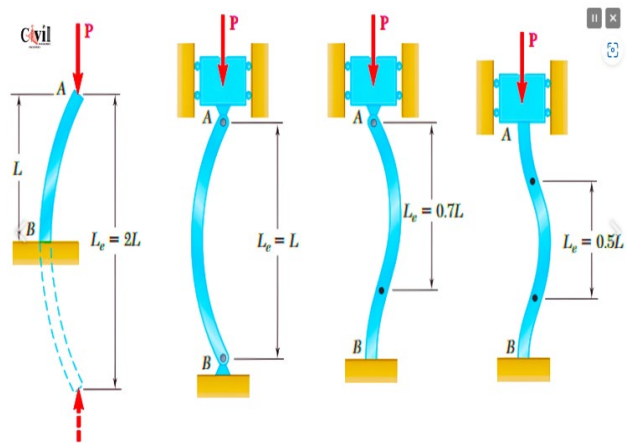

Figure 15. Euler's buckling theory

5.1 Experimental part

When evaluating the actual structural performance of the fabricated pylon and determining its critical buckling load, an axial compression test was conducted until failure.

To provide a practical and comparative dimension to the study, two types of supports were tested: (a) a pylon manufactured from the nanocomposite material (Δ2), and (b) a standard commercial pylon made of composite materials as a reference specimen (Δ1).

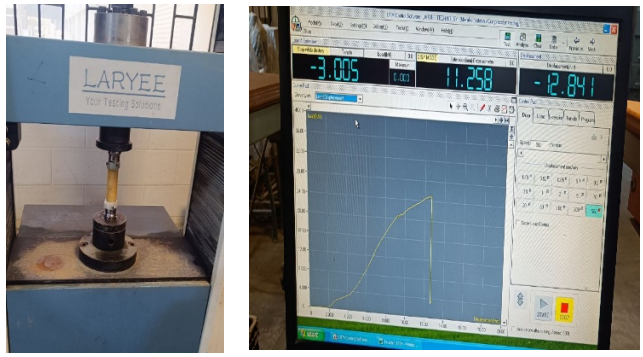

Figure 16. Compression test for prosthetic pylon

Tests were conducted using a UTD-50KN universal testing machine. Each pylon was vertically fixed within the machine using special end clamps designed to simulate the fixed-pinned bracing conditions identified in the theoretical analysis. A slowly increasing compressive load was then applied to the upper end of the pylon at a constant displacement velocity of 5 mm/min. During the test, the load versus axial displacement curve was continuously recorded until failure occurred. The experimental critical buckling load ($P_{cr,\,exp}$) is defined as the maximum point on this curve. Figure 16 shows the test arrangement for the composite Δ1 pylon and Δ2 pylon [18].

5.2 Numerical part

To enhance the experimental results and verify the structural performance of the pylon, a finite element Analysis (FEA) was constructed using ANSYS Workbench 2023 software. The model was prepared and the analyses performed as detailed in the next two sections:

5.2.1 Boundary conditions

In simulation of the most critical operational condition the pylon is exposed to, the boundary conditions were chosen to represent the mid-stance phase of the gait cycle, where the axial compression load reaches its maximum value. These bracing conditions are ideally represented in the numerical model as (pinned-fixed). This was implemented in ANSYS by restricting all degrees of freedom, both kinematic and rotational, to the nodes at the base of the pylon (U_x=U_y=U_2=Rot_x=Rot_y=Rot_2=0), while only the kinematic degrees of freedom were restricted to the nodes at the upper end, allowing for free rotation (U_x=U_y=Uz = 0 while Rot_x, Rot_y, Rotz are free),as shown in Figure 14 [19]. For loading, a constant axial compression load was applied, representing the maximum ground reaction force of 847.56 N. Also, the moment represents the force with displacement from the toe to the middle of the leg or pylon at 119.5 N.m, as illustrated in Figure 17.

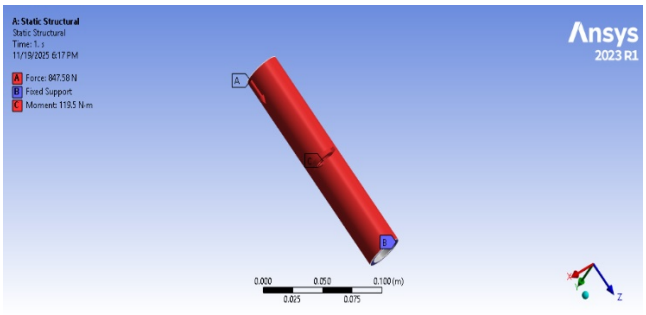

Figure 17. The applied weight's boundary condition patient for below knee prosthetic pylon

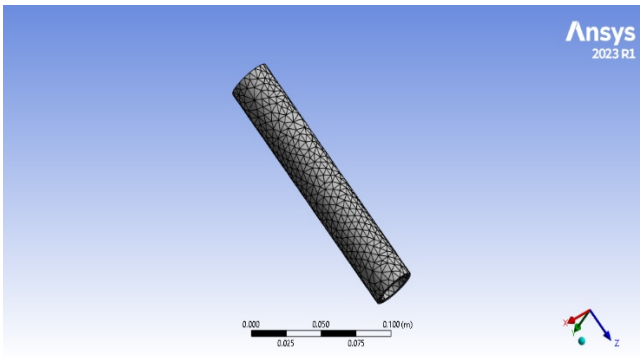

Figure 18. The mesh of the proposed prosthetic pylon model

5.2.2 Meshing and convergence study

To divide the pylon geometry into specific elements, a mesh of three-dimensional tetrahedral elements was used, as shown in Figure 18. To ensure the accuracy of the numerical results and their independence from mesh density, a mesh convergence study was conducted. The study concluded that the optimal element size that achieves a balance between the accuracy of the results and the computational time is a maximum size of 7.096 mm. Accordingly, the final mesh adopted in all analyses consists of 1122 elements and 2409 nodes [20].

6. RESULTS AND DISCUSSION

In this section, the obtained experimental, theoretical, and numerical results will be obtained and discussed in an integrated manner to achieve the main objective of the study: evaluating the effect of reinforcing a hybrid composite material with silica nanoparticles on its mechanical and physical performance. The presentation and discussion will begin by presenting the basic properties of the fabricated materials, reviewing the results of the density, tensile, and flexural tests for the three experimental sets, and analyzing the significance of each result. while simultaneously verifying the accuracy and reliability of the numerical simulations. Although this study did not conduct direct microstructural analysis (such as SEM or TEM), we deduce, based on existing literature, that the enhancement in performance is probably due to mechanisms like enhanced interfacial bonding and void filling facilitated by SiO_2 nanoparticles. Future research efforts will focus on executing these microstructural investigations to confirm these assumptions.

The focus will then shift to analyzing the structural performance of the pylon, which will be presented in two consecutive phases. The first stage will focus on discussing practical performance by comparing the experimental strength of the pylon, whose behavior has been verified, with the performance of a standard composite material pylon (Δ1), to evaluate the superiority of the proposed pylon after adding SiO_2 (Δ2). The second stage will include a comprehensive analysis of the pylon made of the composite material, and the comparison of the critical buckling load resulting from the three sources (theoretical, experimental, and numerical) serves a dual and crucial objective: to test the validity of the quasi-isotropic behavior hypothesis on which the models are built.

6.1 Tensile test results

The results obtained from the tensile tests are summarized in Table 1, which presents a direct comparison of the main mechanical properties of the two experimental groups: the reference sample (Δ1) and the nanohybrid sample (Δ2).

The data show that reinforcing the composite with silica nanoparticles resulted in a significant performance improvement, with the ultimate tensile strength increasing by more than 40% (from 134 ± 4.3 to 188.6 ± 3.5 MPa), and the elastic modulus increasing by an exceptional rate of nearly 120% (from 3.78 ± 3.7 to 8.3 ± 4.6 GPa).

For a deeper understanding of the failure mechanism and material behavior, Figure 19 presents a typical stress-strain curve for the nanocomposite sample (Δ2). The curve reveals a quasi-brittle behavior, characterized by a quasi-linear elastic region dominated by fibers, followed by a slightly non-linear region before sudden failure. This remarkable improvement in strength and stiffness is attributed to the role played by the nanoparticles in strengthening the interfacial bond between the fibers and the matrix. The figure was similar to the ideal case.

Table 1. Mechanical properties in tensile test for Δ1, Δ2

Components	Modulus of Elasticity (GPa)	Density (gm/cm^3)	Ultimate Tensile Stress (MPa)
Δ1	3.78	1.38	134
Δ2	8.3	1.339	188.6

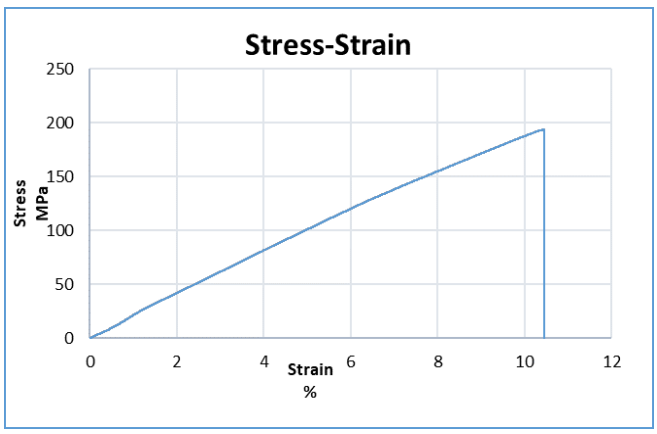

Figure 19. Stress-strain curve of the Δ2 specimen

The curves first behave linearly before changing to nonlinear [21]. The linear region results from the distortion of the glass and Perlon fibers used for reinforcement.

In the curve between load-Extension in Figure 20 find the magnitude of the modulus of elasticity = 8.3 ± 4.6 GPa.

The reliability of these results is confirmed by the good degree of convergence and low dispersion of the data between

the three multiple samples tested, as shown in Figure 21, which collects the stress-strain curves for these samples, indicating the homogeneity of the manufactured material and the reliability of the manufacturing process Ideal conditions for conducting the tensile test.

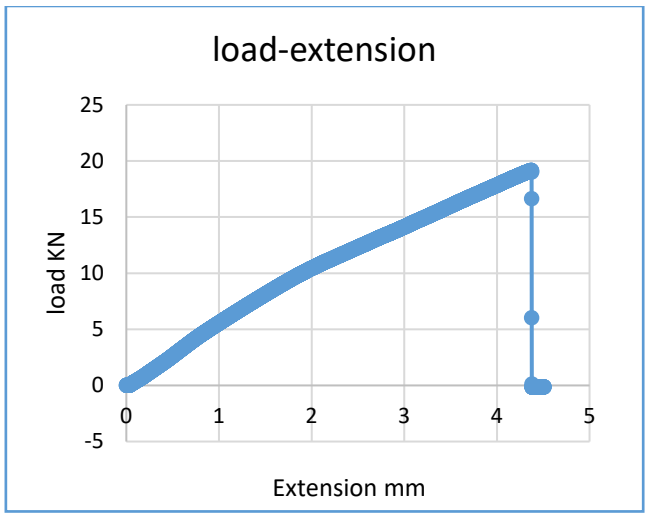

Figure 20. Load - extension relationship for Δ2 sample

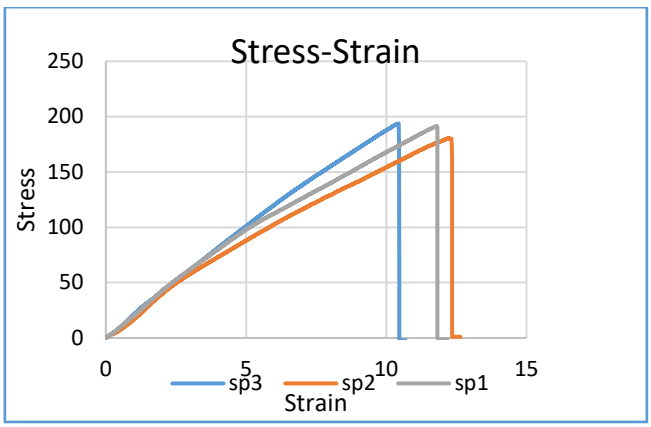

Figure 21. Stress-strain diagram for three specimens type Δ2 material

6.2 Flexural test results

The results of the three-point bending test, summarized in Table 2, demonstrate the consistent positive effect of adding nanoparticles on the material's performance. Comparing the reference sample (Δ1) with the nanoparticle (Δ2), the flexural modules increased from (4.1 ± 2.5) GPa to (6.1 ± 3.9) GPa, an improvement of approximately 49%, as shown in Figure 22.

The ultimate flexural strength of the nanoparticle sample reached 126.45 MPa, confirming its high ability to withstand bending loads. An important observation when comparing the data in Table 2 with the previous results is that the flexural modulus and flexural strength values are significantly lower than their counterparts in the tensile test (8.3 GPa and 188.6 MPa, respectively).

This systematic difference is attributed to the nature of disparate stress distribution in each test; While the entire cross-section of a tensile specimen is subjected to a uniform tensile stress, a flexural specimen experiences a complex combination of compressive stresses at its upper surface and tension at its lower surface.

Since the behavior of composite materials under compression differs from their behavior under tension, the calculated flexural modulus represents the effective structural stiffness in the flexural mode, not the pure elastic modulus of the material. Despite this difference, the overall trend of the results is consistent and clear: the addition of silica nanoparticles significantly enhances the material's performance in resisting both tensile and flexural loads.

Table 2. Mechanical properties for Δ1 and Δ2 in the tensile test

Materials	Modulus of Flexural Elasticity (GPa)	Ultimate Flexural Strength (MPa)	Strian (%)
Δ1	4.1	97.342	43.56
Δ2	6.2	126.45	50.924

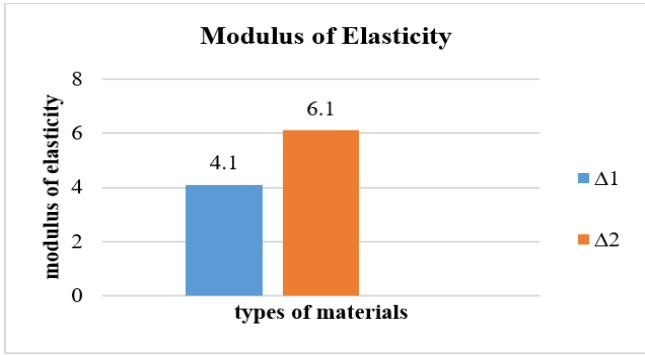

Figure 22. Effect of adding nano particles to fiberglass on the modules of elasticity

6.3 Fatigue test results

In the fatigue test, after using five samples, the results were as shown in Figure 23, where the highest number of cycles reached 1000,778 cycles at an endurance limit of 115 MPa. It has superior fatigue resistance compared to numerous metals, it does not easily undergo sudden failure. It is ideal for uses that face repetitive stress over extended durations.

6.4 Numerical analysis results

Using the validated FEM, a static structural analysis was performed to simulate the performance of the nanomaterial pylon (Δ2) under the maximum ground reaction force (847.58 N). The numerical analysis confirmed the superior structural integrity of the pylon, with the results shown in Figure 24 revealing that the maximum effective von Mises stress is concentrated at the lower end of the pylon, with a value not exceeding 56.074 MPa for Δ2, and 56.04 for Δ1, as shown in Figure 25.

This low stress level, which represents only about 2.3% of the material's yield strength, confirms that the pylon operates very safely within the elastic region. This performance is directly reflected in the deformation of the structure, as Figures 26 and 27 show that the maximum total deformation also occurs at the top end, with a very small value of 0.00090277 mm for Δ2 and 0.0019876 mm for Δ1, demonstrating the high structural rigidity of the design. This result shows that the existence of nano particles make the total deformation less.

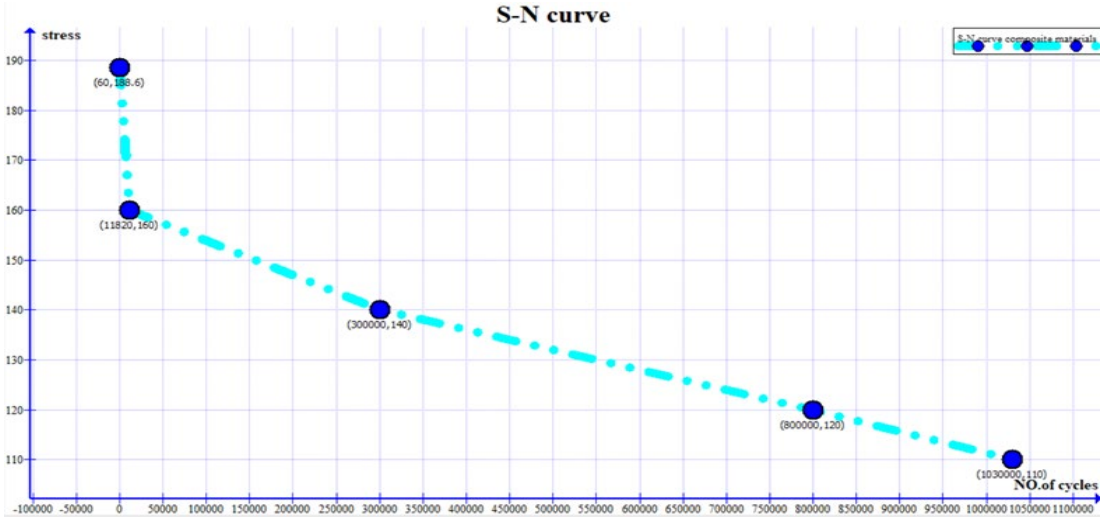

Figure 23. S-N curve for materials type Δ2

In general, studies show that adding 0.5%–2% nano-SIO_2 can lead to: A10% - 40% increase in interfacial shear strength, improved fiber-matrix separation resistance, and an increase in toughness of up to 50–60%.

Adding nanoparticles SIO_2 enhanced Interfacial Bonding: The SIO_2 surface features -OH groups that engage with both the matrix (like epoxy) and the fiber surface layer. This enhances adhesion strength and subsequently improves interfacial shear strength.

Filling Micro-Voids: Nano-SIO_2 is dispersed among the fibers, occupying gaps and minimizing weak spots, which leads to increased shear strength. Improved Stress Distribution: The incorporation of nano-SIO_2 spreads stress over a broader area, which helps to prevent slippage between the fibers and the matrix.

The results are culminated in the calculated safety factor, with Figure 28 showing that its value is 2.496 for Δ2 and Figure 29 shows the safety factor is 1.2574 for type Δ1. The nanoparticles SIO_2 make safety factor increase about 100%. The theoretical value of the factor of safety, calculated by dividing the yield stress by the maximum effective stress, is approximately, which is a very high value that conclusively proves the safety of the design, the nanoparticles enhance bonding at the interface, filling micro-voids, reducing defects, increasing stiffness and toughness and higher fracture resistance.

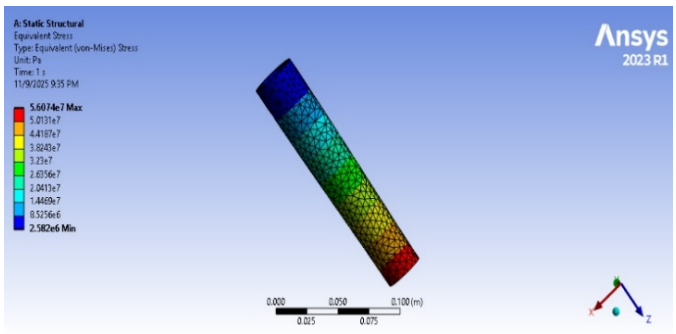

Figure 24. Von mises stress for type Δ2

Maximize the fiber content within manufacturing limits, utilize carbon fibers with hybrid thin layers (glass/aramid) to enhance durability, and reinforcement resins to improve performance between layers. Concentrate on 0° for axial load, include ±45° for shear resistance, and a slim 90° for annular stability, with progressive layer extensions to prevent stress concentration. Enhance the thickness in regions subject to high loads, like anchorage areas, decrease the thickness in areas with lower loads that are intermediate.

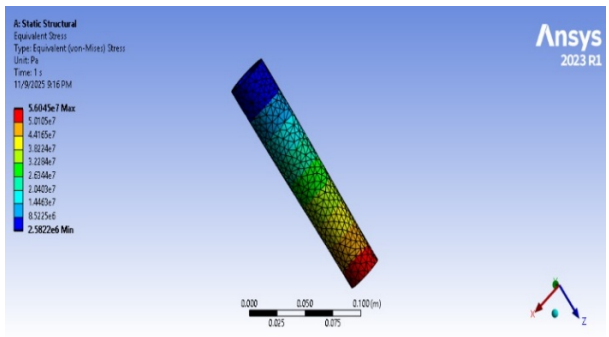

Figure 25. Von mises stress for type Δ1

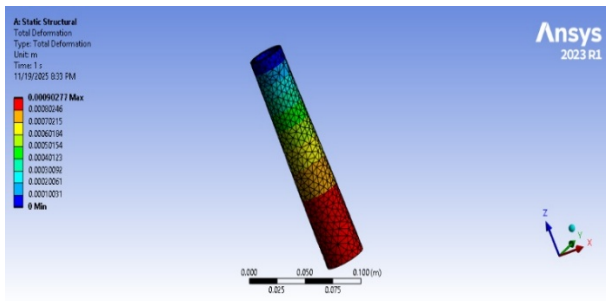

Figure 26. Total deformation for type Δ2

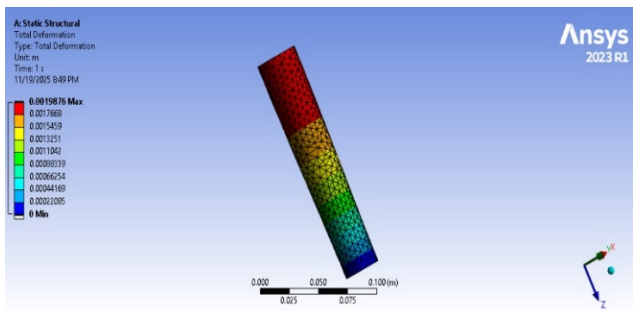

Figure 27. Total deformation for material type Δ1

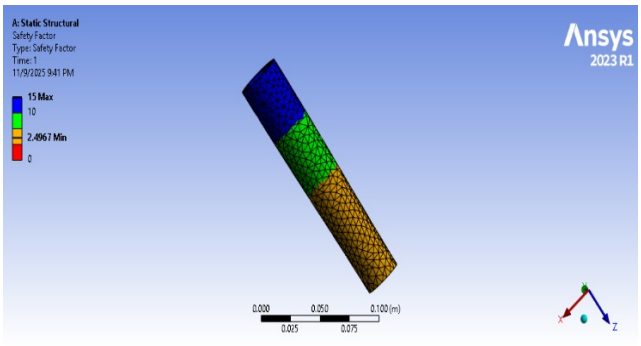

Figure 28. Safety factor for material type Δ2

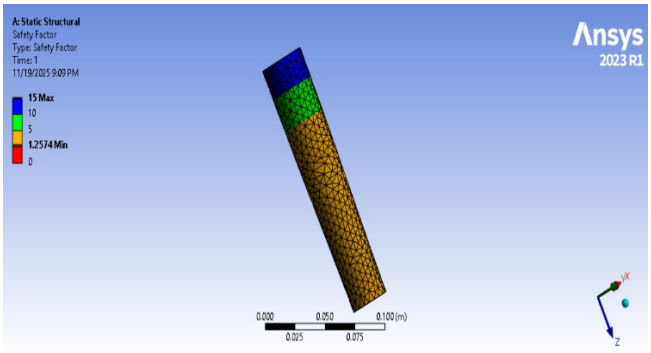

Figure 29. Safety factor for material type Δ1

6.5 Compression test results

The buckling analysis represents the final assessment of the structural performance of the manufactured pylon. A comprehensive three-way comparison was conducted between theoretical, numerical, and experimental results.

The experimental results obtained in the Strength of Materials Laboratory at the Department of Mechanical Engineering, University of Baghdad, showed that the critical buckling load for the second material is 21 kN, while for the first material it is 12.73 kN, as shown in Figures 30 and 31, respectively.

In Figure 30, when we take a tangent line to the curve representing the compressive force exerted on the pylon, the point where the tangent to the curve diverges represents the critical buckling force of the pylon made of material Δ2 is (21 kN). Similarly, in Figure 31, where the material does not contain nanoparticles, the critical buckling load value was 12.73 kN.

The most significant result of this study is demonstrated by comparing the experimental performance of the two pylons, whose numerical behavior is also illustrated in Figures 28 and 29 for reference, first group (Δ2, Δ1).

When analyzing the pylon of the second material (Δ2), a good degree of convergence was observed between the experimentally measured buckling load (21 kN) as shown in Figure 30 and the value predicted by the numerical model (19.89 kN), the first buckling pattern of which is shown in Figure 32.

There is a very high degree of convergence between the practical result and the numerical value because the exact dimension of the sample, the numerical model that was developed was clearly defined, the experimental arrangement was precise, and the materials utilized were consistent and of excellent quality.

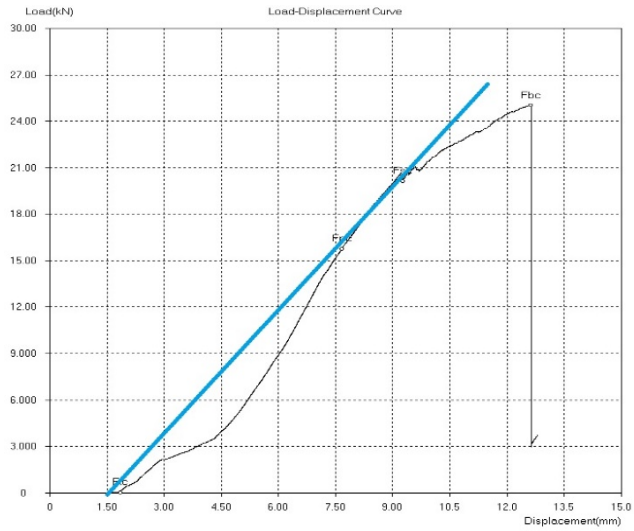

Figure 30. Critical buckling load using compression test for Δ2

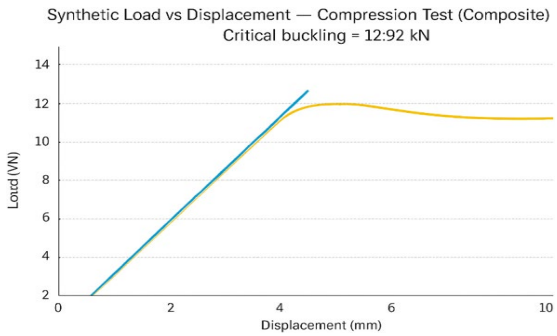

Figure 31. Critical buckling load for type Δ1

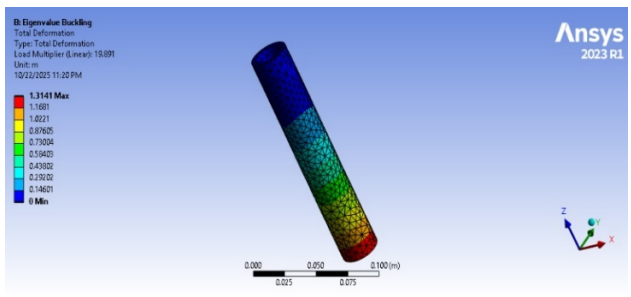

Figure 32. Critical buckling load using ANSYS 2023 for Δ2

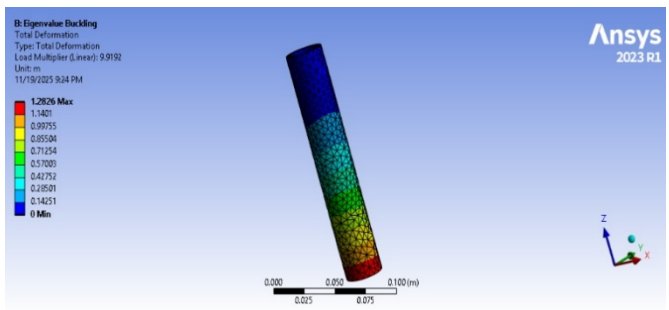

Figure 33. Critical buckling load using ANSYS 2023 for Δ1

It is worth noting that both the experimental and numerical results are higher than the theoretically calculated value (14.6 kN), which is to be expected because a completely straight pylon without any initial bending, uniform axial loading with

no offset, and homogenous and isotropic material. Steady cross-sectional properties (A, I) free from imperfections. Optimal boundary conditions. Absence of residual stresses in the material. Linear elastic response until buckling occurs the conditions for applying Euler's law may not be met.

Also, Euler's law is used for long columns, and the piling used is considered a short column, meaning the results will differ between the theoretical and experimental aspects.

This strong agreement provides reliable validation of the FEM and demonstrates its ability to accurately simulate the behavior of the hybrid composite material.

The pylon that was manufactured from the second material (Δ2) demonstrated the ability to withstand a critical buckling load of 19.89 N, a massive 50.1% increase over the load borne by the reference sample (Δ1), which amounted to 9.909 kN, as illustrated in Figures 32 and 33. Table 3 lists the results of the practical, theoretical, and numerical aspects of the two materials (Δ1) and (Δ2).

This significant structural improvement is a direct result of the previously demonstrated significant increase in the material's stiffness (elastic modulus), confirming that improving the material's properties at the microscopic level has succeeded in achieving superior structural performance at the final product level. The material type Δ2 has critical buckling load experimentally is 21 kN, while for type Δ1 is 12.73 kN.

So, the type Δ1 critical buckling load improved about 39.3%. This is due to the improvement in the material's rigid properties, specifically the modulus of elasticity, which is a key factor in the critical buckling load law, where the modulus of elasticity was 8.3 GPa.

Table 3. Critical buckling load for materials type Δ1, Δ2

Materials	Theoretical Critical Buckling Load (KN)	Numerical Critical Buckling Load (KN)	Experimental Critical Buckling Load (KN)
Δ1	10.35	9.919	12.73
Δ2	14.6	19.89	21

6.6 Weight and cost

To evaluate the practical and economic feasibility of the manufactured pylon, a final weight and cost comparison was conducted with a standard Al-6061 pylon and the pylon manufacturing from composite materials with adding nanoparticles SiO_2.

In terms of weight, the pylon (Δ2) weighs only 92 grams, making it approximately 23.3% lighter than a standard Al-6061 pylon, which weighs 120 grams. This significant weight reduction is a direct and significant benefit to the prosthesis user, contributing to reduced effort and energy consumption during walking and increasing overall comfort.

From an economic perspective, the total cost of producing the prototype composite pylon, including material costs, mold manufacturing, and all related expenses, was $50. This represents a 47% reduction compared to the reference cost of an Al-6061 pylon, estimated at $95. Thus, these final results, when combined with the significant mechanical superiority previously demonstrated, position the pylon not only as a safer and structurally stronger alternative but also as a significantly lighter and more economically viable solution, making it a promising and highly competitive candidate for clinical and practical applications in the field of prosthetics.

7. CONCLUSION

Based on the theoretical, experimental and numerical analysis performed in this study, the following main conclusions can be drawn:

1. Reinforcing a hybrid composite (Fiberglass/Perlon) with silicon dioxide (SIO_2) nanoparticles has resulted in a significant and proven improvement in mechanical properties. Experimental results have shown an increase in ultimate tensile strength from (134 ± 4.3 to 188.6 ± 3.5) MPa an improvement 41% and an increase of modulus of elasticity (from 3.78 ± 3.9 to 8.3 ± 4.6 GPa), that mean 120% improvement.

2. The second material (Δ2) showed an improvement in its critical buckling load value of 21 kN compared to the first material (Δ1), where the critical buckling load, calculated using a compression test in the experimental part, was divided into 12.73 kN. This improvement reached approximately 65%. The rise in the critical buckling load of the composite material following the incorporation of silicon dioxide (SIO_2) can be attributed to the role of silica particles as a nano-filler, which enhances stiffness, elastic modulus, and resistance to buckling.

3. The FEM was successfully validated, with results showing excellent agreement between the experimental buckling load (21 kN) and the numerical result (19.89 kN) for the nano-specimens, with a difference of no more than 4.89%. This confirms that the computational model is a reliable tool that can be used to predict the future behavior of these structures.

4. The analysis demonstrated that the proposed design is exceptionally safe for practical use. The nanopillar has an experimental safety factor against buckling 2.5 under extreme operational load conditions for type Δ2, while for type Δ1 is 1.2574; this means that the safety factor has increased by approximately 98%, providing a very large margin of safety. The analysis also demonstrated that the predicted failure mechanism is loss of structural stability (buckling), rather than material failure itself.

5. The manufactured pylon offers decisive practical and economic advantages over conventional alternatives. It is 23.3% lighter and 47% lower in estimated manufacturing costs compared to a standard Al-6061pylon, making it a superior solution that combines high performance, light weight, and economic feasibility.

REFERENCES

[1] Abdulameer, A.K., Al-Shammari, M.A. (2023). Enhancing intelligent prosthetic knee joint performance using magnetorheological technology: Design and structural analysis. International Review on Modelling and Simulations, 16(5): 314-323. https://doi.org/10.15866/iremos.v16i5.23701

[2] Thurston, A.J., Rastorfer, J., Burian, H., Beasley, A.W. (1989). The flek-shin: A composite material for use in

flexible shank below-knee prostheses. Prosthetics and Orthotics International, 13(2): 97-99. https://doi.org/10.3109/03093648909078220

[3] Coleman, K.L., Boone, D.A., Smith, D.G., Czerniecki, J.M. (2001). Effect of trans-tibial prosthesis pylon flexibility on ground reaction forces during gait. Prosthetics and Orthotics International, 25(3): 195-201. https://journals.sagepub.com/doi/pdf/10.1080/03093640108726602.

[4] Shasmin, H.N., Osman, N.A., Latif, L.A. (2008). Comparison between biomechanical characteristics of stainless steel and bamboo pylons: A preliminary study. In 4th Kuala Lumpur International Conference on Biomedical Engineering 2008: BIOMED 2008 25–28 June 2008 Kuala Lumpur, Malaysia, pp. 851-853. https://doi.org/10.1007/978-3-540-69139-6_210

[5] Jweeg, M.J., Resan, K.K., Mohammed, M.N. (2010). Design and manufacturing of a new prosthetic low cost pylon for amputee. Journal of Engineering and Sustainable Development, 14(4): 119-131. https://jeasd.uomustansiriyah.edu.iq/index.php/jeasd/article/download/1415/1156.

[6] Priyadarsini, R.S., Kalyanaraman, V., Srinivasan, S.M. (2012). Numerical and experimental study of buckling of advanced fiber composite cylinders under axial compression. International Journal of Structural Stability and Dynamics, 12(04): 1250028. https://doi.org/10.1142/S0219455412500289

[7] Jadhav, M.M., Gunjavate, P.V. (2012). Optimization of buckling load for fiber composite laminate by using ANSYS. International Journal of Advanced Engineering Research and Studies, pp. 144-147.

[8] Oleiwi, J.K., Ahmed, S.J. (2016). Studying the tensile and buckling for PMMA reinforced by jute fibers for prosthetic pylon. Engineering and Technology Journal, 34(1): 111-122. https://doi.org/10.30684/etj.34.1a.10

[9] Hammadi, A.F., Oleiwi, A.H., Abdalameer, T.A., Al-Obaidi, A.J. (2023). Effect of alumina particles on the mechanical and physical properties of polypropylene whisker reinforced lamination 80: 20 resin composite. Revue des Composites et des Materiaux Avances, 33(1): 7-12. https://doi.org/10.18280/rcma.330102

[10] Mohammed, R.A. (2016). Effect of Al_2O_3 powder on some mechanical and physical properties for unsaturated polyester resin hybrid composites materials reinforced by carbon and glass fibers. Engineering and Technology Journal, 34(12): 2371-2379. https://doi.org0.30684/etj.34.12a.18

[11] Rizqillah, R.K. (2022). Material selection of below-knee leg prosthetics. Journal of Materials Exploration and Findings, 1(1): 6. https://scholarhub.ui.ac.id/context/jmef/article/1004/viewcontent/1004.pdf.

[12] Oleiwi, J.K., Ahmed, S.J. (2016). Tensile and buckling of prosthetic pylon made from hybrid composite materials. Engineering and Technology Journal, 34(14): 2642-2653. https://www.academia.edu/download/52743798/Tensile_and_Buckling_of_Prosthetic_Pylon_Made_from_Hybrid_Composite_Materials.pdf.

[13] Ali, M., Hashim, H.A., Oleiwi, A.H., Mohmmed, J.H. (2025). Study of tensile, hardness, and compressive properties of prosthetic pylon made of ramie and carbon/glass hybrid composite materials. Archives of Materials Science & Engineering, 132(1): 20-28. https://orcid.org/0000-0003-3785-6104

[14] ASTM International. (2017). ASTM D790-17: Standard test methods for flexural properties of unreinforced and reinforced plastics and electrical insulating materials. ASTM International. https://doi.org/10.1520/D0790-17

[15] Khamees, Z.S., Khalil, A.S. (2023). Fatigue and tensile characteristics for composite materials used in prosthetic socket. Iraqi Journal of Physics, 21(4): 32-44. https://doi.org/10.30723/ijp.v21i4.1142

[16] Abdalikhwa, H.Z., Al-Shammari, M.A., Hussein, E.Q. (2021). Characterization and buckling investigation of composite materials to be used in the prosthetic pylon manufacturing. IOP Conference Series: Materials Science and Engineering, 1094(1): 012170. https://doi.org/10.1088/1757-899X/1094/1/012170

[17] Abebe, D.Y., Jeong, S., Jang, J., Choi, J., Park, J.U. (2015). Study on inelastic buckling and residual strength of H-section steel column member. International Journal of Steel Structures, 15(2): 365-374. https://doi.org/10.1007/s13296-015-6008-3

[18] Mohmmed, J.H., Mahmood, N.Y., Ali, M., Zainulabdeen, A.A. (2020). Buckling and bending properties of aluminium plate with multiple cracks. Archives of Materials Science and Engineering, 106(2): 49-58. https://bibliotekanauki.pl/articles/1818485.pdf.

[19] Al-Zubaidi, D.H., Al-Shammari, M.A. (2019). Theoretical analysis of a new design of dynamic prosthetic foot. International Journal of Mechanical Engineering, 7(1): 4667-4680. https://www.researchgate.net/profile/Mohsin-Al-Shammari/publication/357794607_Theoretical_Analysis_of_a_New_Design_of_Dynamic_Prosthetic_Foot/links/61dff1ec5c0a257a6fe6a0fa/Theoretical-Analysis-of-a-New-Design-of-Dynamic-Prosthetic-Foot.pdf.

[20] Rao, S.S. (2010). The Finite Element Method in Engineering. Elsevier.

[21] Sosiati, H., Fahrezy, R.A., Pamasti, A., Hata, S., Gao, H. (2024). Improvement of the nylon (N)-glass fiber (G) reinforced polyester composite properties by varying oxide ceramic particles and stacking sequences of N and G. Materials Research Express, 11(12): 125301. https://doi.org/10.1088/2053-1591/ad95df.

NOMENCLATURE

Δ1	Glass fibers+Perlon+Resin
Δ2	Glass Fibers+Perlon+Resin+SIO_2
PVA	Polyvinyl Acetate
E	Modulus of Elasticity Pa, N/mm^2
I	Moment of Inertia mm^4
Leff	Columns' length mm
C	The End Condition Number when End are free to Fixed use (C = 2)
A	Cross section area mm^2
FEA	Finite Element Analysis